Available online at www.sciencedirect.com
ScienceDirect
Journal of Nuclear Materials 362 (2007) 493–501
journal of nuclear materials
www.elsevier.com/locate/jnucmat

Modelling glass alteration in an altered argillaceous environment

O. Bildstein *, L. Trotignon, C. Pozo, M. Jullien

CEA DTN/SMTM/LMTE – CE Cadarache, 13108 St. Paul lez Durance, France

Abstract

The long term behaviour of materials such as glass, steel and clay has been investigated in the context of deep geological disposal of radioactive wastes. The interactions between vitrified wastes, canister corrosion products (CPs) and clay are studied using a modified version of the reaction-transport code Crunch, especially looking at pH changes and possible cementation at the interface with the clayey materials. These perturbations may indeed affect the lifetime of glass matrix in deep repositories, e.g., high pH enhances the rate of glass alteration. This work focuses on the argillite of Bure. The calculations were performed at 323 K with a glass alteration rate switching from a high initial rate to a residual rate according to the sorption capacity of CPs. The time at which this sorption capacity is saturated is crucial to the system in terms of wastes package lifetime. The results show that the glass alteration imposes a high pH value at the interface with CPs and clay: up to a value of 9.2, compared to 7.3 which is the initial pH value in the argillite. Experimental data show that the rate of glass alteration is much higher in such pH conditions. For a R7T7-type glass, the rate is about five times higher at pH 9 than at pH 7. This pH perturbation migrates through the clayey domain as a result of the migration of mobile elements such as boron and sodium, and despite the existence of strong pH buffers in the argillite. The cementation of porosity at the interface between glass and clay is predicted by the model due to the massive precipitation of iron corrosion products and glass alteration products. At this point of the evolution of the system, the pH starts to decrease and the alteration rate of the glass could be significantly reduced. This porosity clogging effect is difficult to confirm by experiments especially since existing data on short term experiments tend to show a pervasive precipitation of silica in the domain instead of a localized precipitation at the interface.

PACS: 02.60.Cb; 82.20; 82.30; 82.40; 91.65.Fw; 91.65.Vj; 92.20.Mx; 92.40.Kf; 92.60.Hp

1. Introduction

The interactions between glass, steel and clay are investigated in the context of deep geological disposal. The evolution of near field (NF) and especially the precise nature and properties of the materials in contact with glass when the canisters will fail is crucial to the lifetime of the waste packages.

After closure of the repository, the region close to the waste packages, also called the near field system, will progressively resaturate and the corrosion of the canisters will start, releasing substantial amounts of iron in reduced conditions. A variety of iron oxides, oxy-hydroxides and carbonates may precipitate (such as magnetite and siderite) as

* Corresponding author. Tel.: +33 442253724; fax: +33 442256272.
E-mail address: olivier.bildstein@cea.fr (O. Bildstein).

0022-3115/$ - see front matter © 2007 Elsevier B.V. All rights reserved.
doi:10.1016/j.jnucmat.2007.01.225

well as new Fe-rich phases forming at the expense of the initial clay minerals. The former products are crucial to the behaviour of silica released by glass and therefore on the alteration rate of glass. The latter products are responsible for potential adverse modifications in the cation exchange capacity (CEC), the swelling capacity, and possibly the mechanical and transport properties of the barriers [1].

2. Near field description and model

The calculations of the NF evolution include the vitrified waste package, the steel container, the excavation damaged zone (EDZ) and the geological medium. The presence of a bentonite-based engineered barrier system (EBS) is considered an option for the disposal of vitrified wastes but the results obtained this system will not be presented here.

2.1. The reactive transport model

A modified version of the coupled reaction-transport code Crunch [2] is used to calculate the corrosion of the steel canister and the glass alteration phase in presence of corrosion products (CPs), looking at mass transfer for chemical elements, especially iron and silica, the pH evolution in the system, and the porosity changes especially in the cells containing the glass matrix and the steel container.

The modifications of the code concern mainly the handling of the alteration rate of the NF materials including:

- a strictly constant rate and surface area for corrosion of the steel canister, i.e., these parameters do not vary even if porosity varies,
- time lapse before glass is altered (only after a certain amount of steel is corroded), and then a specific '$r_0 \rightarrow r_r$' glass alteration rate is applied (see Section 3.1).

Crunch takes into account the entire range of transient and steady-state phenomena, including advection, dispersion, and diffusion transport. The code uses a kinetic formulation for all mineral dissolution and precipitation reaction. In this application, the aqueous complexation reactions (including redox) are assumed to be reversible, i.e., are considered at equilibrium. The governing equation for the conservation of the mass of a chemical element j is given by

$$\frac{\partial}{\partial t}(\phi\rho_f M_{H_2O} C_j) + \nabla\cdot\left[u\rho_f M_{H_2O} C_j - D\nabla\left(\rho_f M_{H_2O} C_j\right)\right] = R_j^{min} \quad (j = 1,\ldots,N_c), \tag{1}$$

where C_i is the total molal concentration of element j in solution (mol kg^{-1}), M_{H_2O} is the mass fraction of H_2O (–), ρ_f is the fluid volatile density (–), u is the Darcian flux (m a^{-1}), D is the combined dispersion–diffusion tensor (see Section 2.2), R_j^{min} is the total mineral reaction rate of element j in solution (mol a^{-1}), and N_c is the total number of components (chemical elements). The terms on the left hand side represent respectively the accumulation, advection, and diffusion contributions to the conservation of the chemical element mass. In this paper, only diffusion is considered to occur in the argillites.

The generic formulation of the kinetic law is based on the theory of the transition state law which was developed by Lasaga [3,4] and Aagaard and Helgeson [5]:

$$v_m = k_m(T) S_m (a_i)^{n_i}\left(1 - \frac{Q_m}{K_m(T)}\right), \tag{2}$$

where v_m is the mineral kinetic rate of reaction (mol a^{-1}), $k_m(T)$ the kinetic constant (mol m^{-2} a^{-1}), S_m the reactive surface area (m^2), $(a_i)^{n_i}$ an inhibition/catalysis factor (–), Q_m the ionic activity product, and $K_m(T)$ the equilibrium constant. Data for the equilibrium calculations in the aqueous phase are taken from the EQ3/EQ6 database [6]. The kinetic constant depends on temperature according to the Arrhénius' law:

$$k_m(T) = k_m(298)\exp\left[-\frac{E_{ap}}{R}\left(\frac{1}{T} - \frac{1}{298}\right)\right], \tag{3}$$

where T is the temperature (K), E_{ap} the activation energy of the dissolution/precipitation (ap) reaction (J mol^{-1}), and R the perfect gas constant (J mol^{-1} K^{-1}). The kinetic parameters for mineral dissolution and precipitation are given in Table 3.

2.2. System studied

The system is modelled using a 1D purely diffusive, fully saturated multi-domain, open for diffusive exchange with water from the host-rock. It includes a 15 cm thick glass package, a 7 cm thick steel canister and 10 m of argillite. The calculations

were performed at 323 K, which is considered a mean value in the glass alteration phase of the repository lifetime.

The surface area of the clay interface is 1 m^2 for the cartesian system. The simplified glass composition is based on the R7T7 reference glass but with five oxides only: 45.5% Si, 14.0% B, 9.9% Na, 4.9% Al, and 4.0% Ca (in wt% of oxides). The stainless steel canister is composed only of iron.

The initial mineralogical composition and porosity of the Callovo-Oxfordian argillites are given in Table 1. The water composition is calculated using both mineral equilibrium constraint and in situ measurements (Table 2) and compares closely with measurements from the Bure site [7,8].

Table 1
Simplified composition of the Callovo-Oxfordian argillites of Bure

Minerals	Volume fraction (%)	Surface area per rock volume (m^{-1})
Illite	30.2	10^5
Montmor-Ca	9.4	10^5
Montmor-Na	3.5	10^5
K-Feldspar	1.8	0.01
Kaolinite	0.4	1
Quartz	22.0	1
Calcite	14.6	1
Pyrite	0.5	0.01
Goethite	0.3	0.01
Dolomite	2.4	0.0001
Porosity	14.9	–

Table 2
Water composition of the Bure argillites at 298 K

	Value calculated	Constraint used
Total element concentration (mM)		
Na	68.8	Na-Montmorillonite
K	10.4	Illite
Mg	0.3	Dolomite
Ca	3.4	Ca-Montmorillonite
Si	0.4	Chalcedony
Cl	20.0	From measurements
SO_4	30.0	From measurements
CO_3	7.7	Calcite
Al	1.9×10^{-5}	Kaolinite
Fe	1.8×10^{-2}	Pyrite
pH	6.9	From measurements
B	10^{-12}	Imposed concentration
$Log O_2$ (aq)	−63.7	Magnetite
Calculated parameters		
pCO_2 (bar)	9.2×10^{-2}	
Eh (mV)	−164	
Ionic strength (mM)	113	

No boron is initially present in the water.

A difficulty arises with common reactive transport models which cannot account for non-porous media such as glass and steel: the cells containing the glass matrix and steel canister have to be modelled as porous media, i.e., they have to contain water. In the real system, a volume clearance exists at the interface between the canister and the clayey material, which is referred to as the technological gap. In the model, the 'canister cell' is thus represented as a 17 cm thick cell which contains the steel canister, a technological gap and a fraction of clay (host-rock argillite). A 3 cm technological gap is also considered in the cell containing glass. These technological gaps are also introduced in the simulations to accommodate the volume occupancy of corrosion products and the potential swelling of clays. This latter phenomenon, as well as the resulting mechanical stress, is not accounted for in the present model.

The porosity is updated according to the net volume balance of dissolved and precipitated minerals. The code is given a single molecular diffusion coefficient at 298 K for all the aqueous species ($D_0 = 10^{-9}$ m^2 s^{-1}) and an activation energy E_{ad} for the diffusion (ad) process ($E_{ad} = 13.8$ kJ mol^{-1}) [9]. The effective diffusion coefficient, D_{eff}, is calculated as a function of the porosity and updated during the simulation using Archie's law (Archie [10]; see application to diffusion coefficients by Norton and Knapp [11]; Skagius and Nieritnieks [12]; Nakashima [13]):

$$D_{eff} = D_0 \exp\left[\frac{-E_{ad}}{R}\left(\frac{1}{T} - \frac{1}{298.15}\right)\right]\phi^m, \quad (4)$$

where ϕ is the porosity (–), m is the cementation factor (–), and R is the perfect gas constant (kJ mol^{-1} K^{-1}). The cementation factor reflects the tortuosity in a porous material which affects the transport of dissolved species, a decrease in porosity resulting in an exponential decrease of the diffusion coefficient. The value of m is determined by fitting the effective diffusion coefficient measured at the Bure site [7]: $\phi = 15\%$ and $D_{eff} = 10^{-11}$ m^2 s^{-1} give $m = 2.5$, considering a temperature of 298 K. This value is consistent with other studies on clayey materials [13–15].

2.3. Canister corrosion rate and corrosion products

As a result of steel corrosion, the pH increases, high amounts of iron are released in the system forming iron oxides, oxy-hydroxides and carbonates

Table 3
Kinetics parameters for mineral precipitation and dissolution at 298 K

Minerals	Formula	Kinetic constant $\log k_m$ (mol m^{-2} s^{-1})	Refs.
Na-montmorillonite	$Na_{0.33}(Mg_{0.33},Al_{1.67})Si_4O_{10}(OH)_2$	−12.8	[23]
Ca-montmorillonite	$Ca_{0.165}(Mg_{0.33},Al_{1.67})Si_4O_{10}(OH)_2$	−12.8	[23]
K-feldspar	$KAlSi_3O_8$	−11.5	[24]
Albite	$NaAlSi_3O_8$	−13.0	[25]
Chalcedony	SiO_2	−13.5	[26]
Calcite	$CaCO_3$	−6.2	[27]
Pyrite	FeS_2	−5.3	[28]
Illite	$K_{0.75}(Al_{1.75},Mg_{0.25})(Si_{3.5},Al_{0.5})O_{10}(OH)_2$	−12.8	[23]
Kaolinite	$Al_2Si_2O_5(OH)_4$	−13.0	[29]
Quartz	SiO_2	−14.0	[30]
Goethite	$FeO(OH)$	−9.0	[31]
Siderite	$FeCO_3$	−9.0	[31]
Dolomite	$Mg(CO_3)_2$	−7.7	[32]
Cronstedtite	$(Fe^{2+}_2,Fe^{3+})(Si,Fe^{3+})O_5(OH)_4$	−12.8	[23]
Chamosite	$(Fe^{2+}_2,Al)(Si,Al)O_5(OH)_4$	−12.8	[23]
Mg-saponite	$Mg_{0.165}(Mg_3)(Si_{3.67},Al_{0.33})O_{10}(OH)_2$	−12.8	[23]
Mordenite	$(Ca_{0.32},Na_{0.36})AlSi_5O_{12}$	−14.0	[a]
Natrosilite	$Na_2Si_2O_5$	−14.0	[a]
Borax	$Na_2B_4O_5(OH)_4 \cdot 8(H_2O)$	−14.0	[a]

Kinetic constants at 323 K are calculated considering an activation energy of 60 kJ mol^{-1} (surface reaction controlled kinetics).
[a] Borax, natrosilite, and mordenite were used as sinks for different elements in the glass for which a slow rate was used as compared to the other secondary minerals.

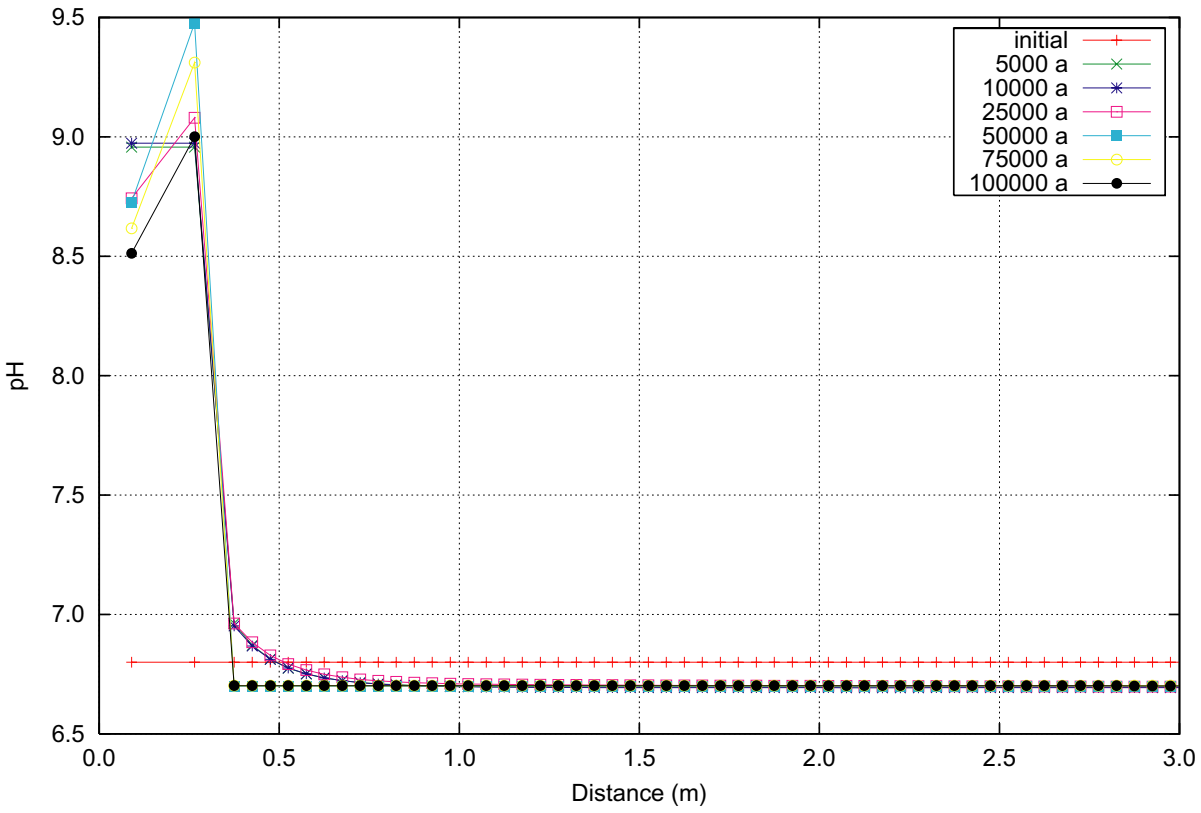

Fig. 1. pH evolution with time at the glass–steel, steel–EDZ interfaces and into the site (zoom over 3 m).

(such as magnetite and siderite). The interactions with clayey materials also form new 7 Å Fe-rich phases due to the alteration of primary clay minerals which are iron-rich serpentines such as berthierine and cronstedtite ([16,1]; and references therein). A constant corrosion of 4.3 μm a^{-1} was considered in the reference case at 323 K [17].

The most important impact of the nature of corrosion to be considered for the alteration of glass is the immobilisation, potentially both sorption and precipitation of silica, at the surface of metallic iron and CPs. Indeed, this process affects the silica concentration at the interface between the glass matrix and the altered canister thus controlling the glass alteration rate. This is a key point in the operational model of glass alteration currently used at the CEA since the switch from the high initial rate to the residual rate occurs precisely when the sorption sites of CPs are fully saturated with silica. With these data, a mass balance calculation shows that if the total volume of steel is corroded into magnetite, the saturation time would lie between 5 and 250 years based on glass alteration rates at 323 K (depending on pH); twice as much time if the main CP is siderite (see sorption capacity in next section).

In the absence of a full understanding on the behaviour of aqueous silica in the system, pure sorption or sorption followed by precipitation of silica [18], an irreversible sorption capacity on PCs will be considered in the following calculations. The model calculates the total sorption capacity on the CPs, at any time during the simulation, and compares the value with the amount of silica released by the alteration of glass.

2.4. Glass alteration rate

According to the operational model used at the CEA for performance assessment calculations the alteration of glass proceeds in two stages [19]:

– An initial stage during which the rate of alteration r_0 is high, and depends on pH and temperature:

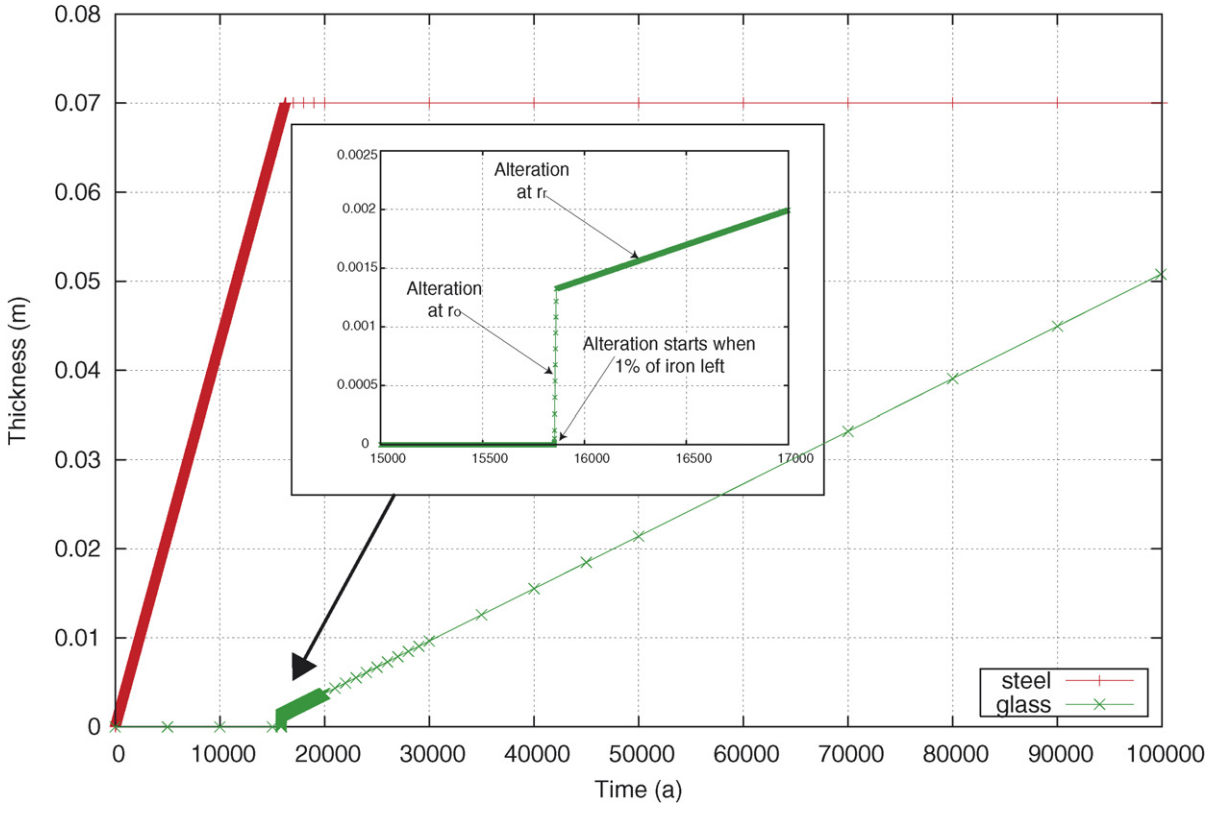

Fig. 2. Thickness of altered glass and steel as a function of time. *Note*: corrosion rate is constant; the glass alteration starts when the canister fails and proceeds in two sequential regimes: $r_0 \rightarrow r_r$.

$$r_0 = r_{0T_0} \exp\left(-\frac{E_{a0}}{R}\left[\frac{1}{T}-\frac{1}{T_0}\right]\right) 10^{N_0 f(\mathrm{pH})} \quad (5)$$

with $T_0 = 373$ K, $E_{a0} = 76$ kJ mol^{-1}, $N_0 = 0.4$, and $r_{0T_0} = 1.7$ g m^{-2} d^{-1} (subscript 0 standing for 'initial stage') and $f(\mathrm{pH}) = \mathrm{Max}\ (\mathrm{pH} - 7; 0)$, which specifies that the glass alteration rate is affected by pH only when pH is higher than 7.

– A final stage during which the alteration rate has reached a low residual rate, r_r (subscript r standing for 'residual stage') only depending on temperature:

$$r_r = r_{rT_r} \exp\left(-\frac{E_{ar}}{R}\left[\frac{1}{T}-\frac{1}{T_r}\right]\right) \quad (6)$$

with $T_r = 323$ K, $E_{ar} = 53$ kJ mol^{-1}, and $r_{rT_r} = 6 \times 10^{-5}$ g m^{-2} d^{-1}.

The 'reactive' surface area of glass also depends on the regime of alteration through a fracture ratio (τ) which increases the geometrical surface area: $\tau_0 = 5$ in the initial regime and $\tau_r = 40$ in the residual regime.

The glass alteration rate switches from one regime of alteration to the other according to the reactivity of the environment, i.e., the ability to maintain a low concentration of aqueous silica at the interface with the glass. This reactivity is thought to be supported either by the products of the canister corrosion (CPs) adsorbing a high quantity of silica, or by clay minerals in the EBS and argillites in direct contact with glass. In these calculations, the silica is considered to be sorbed mainly on the CPs as follows: 160 μg of silica per gram of magnetite and 190 μg per gram of siderite [20].

In the following calculations, the switch between initial and residual regime is considered to occur instantaneously, when silica sorption reaches the sorption capacity of PCs (saturation). This is assumed essentially because of the lack of parameters describing the gradual decrease of the alteration

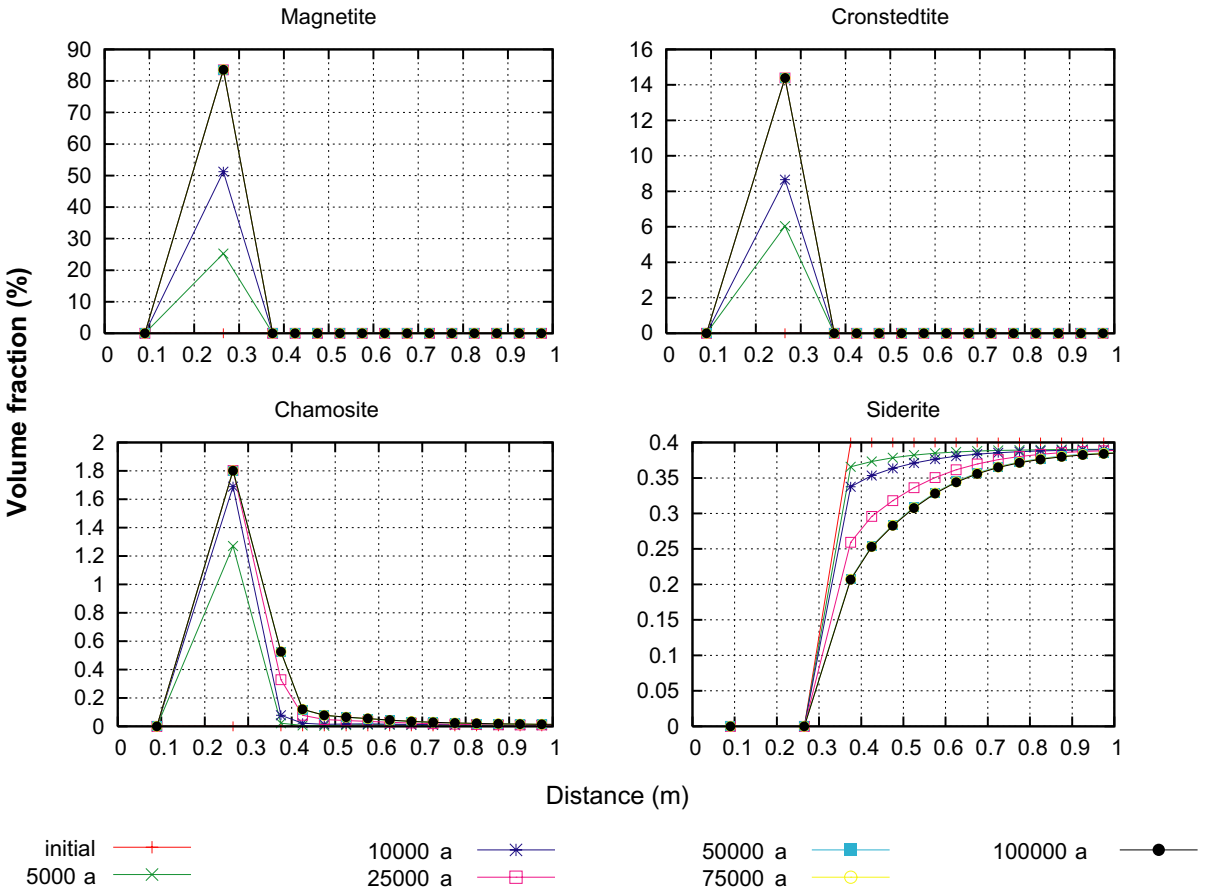

Fig. 3. Distribution of corrosion products. *Note*: the steel canister corrodes forming 80% magnetite and 14% cronstedtite, siderite does not precipitate.

rate with time in the conditions of the repository, i.e., concerning the 'reactivity' of the different materials with respect to glass alteration.

As a conservative hypothesis, the glass is altered at the initial alteration rate r_0 during this reactive stage, the switch to the residual rate r_r occurring only when the physical/chemical 'immobilisation' capacity of silica of the materials in the NF is reached.

The alteration of glass leads to the release of major species (silica, boron, sodium) and secondary species (calcium, aluminium), and to a significant increase in pH. This perturbation will affect the minerals from the EBS and the site, dissolving primary minerals and precipitating secondary phases. Some porosity clogging may also be expected due to the sorption/precipitation of silica mineral phases on the surface of CPs and the precipitation of silica minerals (such as amorphous silica and chalcedony) in the clay matrix.

3. Results and analyses

The calculation takes into account the direct interaction between glass and steel with the argillite (case without EBS) over a period of 100 000 a. The 7 cm steel canister corrodes at a constant rate of 4.3 μm a^{-1}. When 99% of the corrosion is completed (i.e., ~16 200 a), the canister looses its integrity, water enters the canister and the alteration of glass begins. The corrosion of the canister proceeds simultaneously with glass alteration until complete corrosion of the canister. The code automatically switches from alteration rate r_0 to r_r after 10 years of alteration, which is the time needed for the CPs to become saturated with silica (see Fig. 2). The porosity drops dramatically in the canister cell after 6000–16 000 a, due mainly to the precipitation of CPs. Due to the feedback with the diffusion coefficient, the transport of aqueous species is therefore limited at this location.

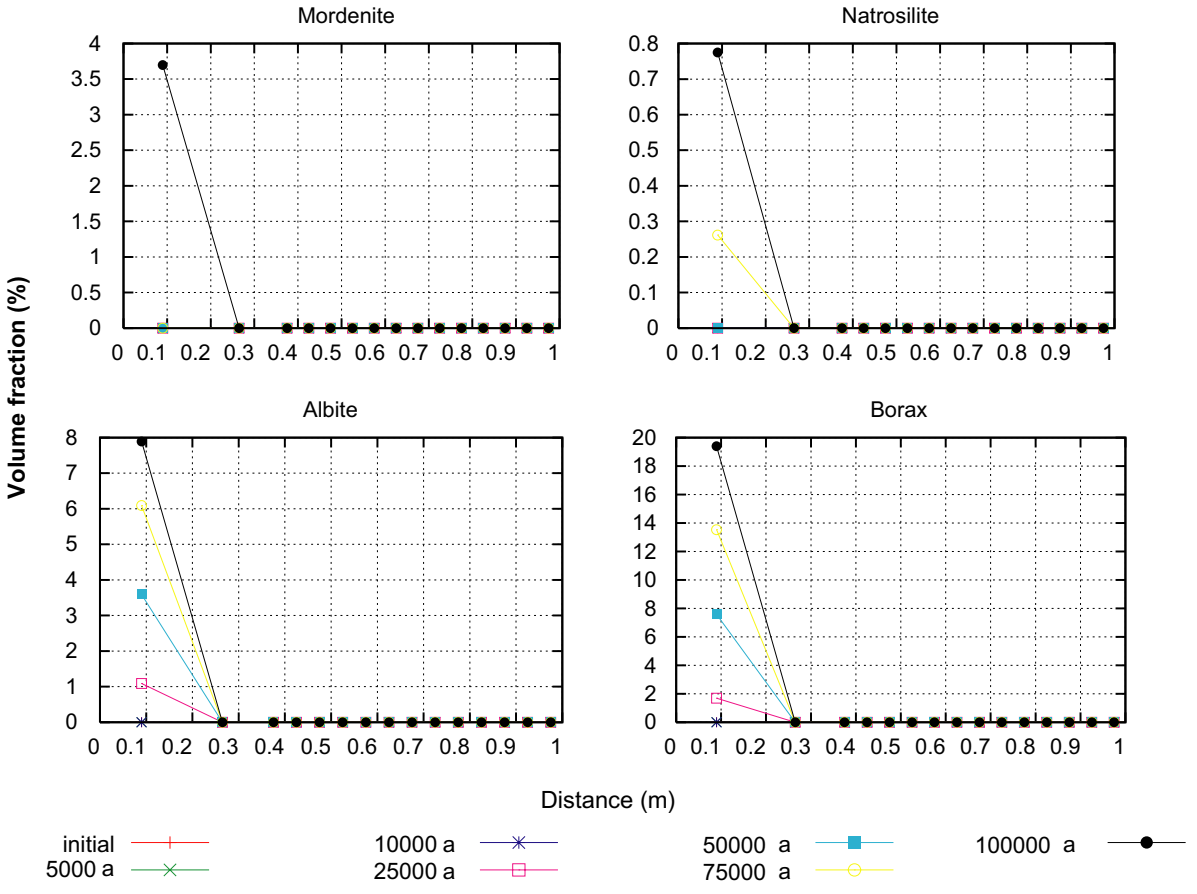

Fig. 4. Distribution of glass alteration products. *Note*: zeolite-type minerals precipitate (composition close to a gel phase) as well borax and albite as sinks for boron and sodium.

3.1. pH evolution and glass alteration rate

The pH at the interface between glass and steel stabilizes at a value around 9.0 during corrosion stage and when the alteration of glass starts (Fig. 1). Note that in this calculation, the pH perturbation is limited to the first ca. 50 cm in the domain. In the initial stage, the glass alteration rate is $r_0 = 0.20\ \mathrm{g\ m^{-2}\ d^{-1}}$ for a short period of time (ca. 10 a) which is the time needed to saturate the CPs with sorbed silica. After this stage, the alteration rate of glass decrease to a constant value $r_r = 0.0008\ \mathrm{g\ m^{-2}\ d^{-1}}$. This behaviour is supported by experiments showing that the residual rate is still established even if the pH value is high when glass alteration starts [21]. At this rate, a third of the volume of glass is altered in 100 000 a (Fig. 2).

3.2. Mineralogical and porosity evolution

The complete corrosion of the canisters takes 16 200 a (Fig. 2). In this simulation, the main CPs forming are magnetite, cronstedtite and chamosite (<2%) and no siderite has precipitated (Fig. 3). Furthermore, the siderite is destabilized in the argillites by the precipitation of calcite at the interface with the canister. The high pH and massive precipitation of magnetite seem to prevent siderite precipitation. The simulations also predict that the porosity drops dramatically in the canister cell due to the precipitation of magnetite (80% of the canister cell volume) and cronstedtite (14% of the canister cell volume).

The main products of the glass alteration predicted by the model are Albite (8%) and Borax (20%) (Fig. 4) which were introduced as sinks for boron and sodium. The high stability of Albite prevents other mineral such as zeolites from forming. Zeolites are observed in natural and archaeological analogues as glass alteration products. The composition of these minerals is close to the gel surrounding the glass during alteration. In these calculations, only 4% Mordenite (a Na, Ca–zeolite) is precipitating. Borax is the only boron bearing mineral for which thermodynamical data are available in the database at temperatures higher than 298 K (data at 298 K are available for other hydrated calcium borate hydroxide minerals, such as Colemanite, or hydrated calcium magnesium borate, such as Hydroboracite). These results raise the question of the secondary minerals to be accounted for in the simulations. A sensitivity analyses would be necessary to assess the influence of the precipitation of other zeolites, and in general of other aluminosilicate phases.

4. Conclusions

According to the operational model currently used at the CEA and the calculations performed on the glass–iron–clay system, the alteration rate of glass and the evolution of the system strongly depend on the timing for the CPs sorption sites to be saturated with silica. In these calculations, CPs are saturated in ~10 years leading to a negligible amount of glass alteration at a high initial rate (1 mm altered out of the 15 cm). In these conditions, the alteration of glass mainly takes place at a low residual rate (one third of the glass altered in 100 000 years). Since the time needed for the sorption capacity to be saturated is so crucial to the system, there is a need for more understanding of the mechanisms of immobilisation of silica on CPs and on metallic iron, and for more reliable data on this process.

The other process that might prevent the glass from being altered rapidly is the porosity clogging due to the precipitation of CPs and silica rich phases. Clogging can be regarded as a favourable process for performance assessment but is scarcely observed in experiments, either because it does not occur or because the timescale of this process is not accessible to experiments. The role of clogging has also to be assessed with regard to mechanical stress, e.g., shear stress, with might prevent any protective function from being effective on the long term. The complexity of the mechanisms at play when the porosity is vanishing due to geochemical interactions in a porous media calls for further theoretical and experimental investigation [22].

Acknowledgements

Part of this work has been performed under the auspices of the EC-EURATOM 6th Framework Program Integrated Project NF-PRO (Near Field Processes). We acknowledge fruitful discussions with I. Ribet, N. Godon, J.E. Lartigue and G. de Combarieu (CEA, Marcoule), as well as the technical support from Carl Steefel (LBNL, USA), the author of the reaction-transport code used in this paper. We also acknowledge three anonymous reviewers for thoughtful comments on this paper.

References

[1] O. Bildstein, L. Trotignon, M. Perronnet, M. Jullien, Phys. Chem. Earth 31 (2006) 618.
[2] C.I. Steefel, CRUNCH: Software for modeling multicomponent, multidimensional reactive transport, User's Guide, UCRL-MA-143182, Livermore, California, 2001.
[3] A.C. Lasaga, Rev. Miner. 4 (1981) 135.
[4] A.C. Lasaga, J. Geophys. Res. 89 (1984) 4009.
[5] P. Aagaard, H.C. Helgeson, Am. J. Sci. 282 (1982) 237.
[6] T.J. Wolery, Lawrence Livermore Nat. Lab. Report UCRL-MA-110662 PT IV, Livermore California, USA, 1992.
[7] Andra, Dossier 2005 – Argile (2005). Available from: <www.andra.fr>.
[8] E. Gaucher, C. Robelin, J.M. Matray, G. Negral, Y. Gros, J.F. Heitz, A. Vinsot, H. Rebours, A. Cassagnabere, A. Bouchet, Phys. Chem. Earth 29 (2004) 55.
[9] Y.H. Li, S. Gregory, Geochim. Cosmochim. Acta 38 (1974) 703.
[10] G. Archie, Trans. AIME 146 (1942) 54.
[11] D. Norton, R. Knapp, Am. J. Sci. 277 (1977) 913.
[12] K. Skagius, I. Nieritnieks, Water Resour. Res. 22 (1986) 389.
[13] S. Nakashima, Tectonophysics 245 (1995) 185.
[14] M. Manaka, M. Kawasaki, Nucl. Technol. 130 (2000) 206.
[15] L.R. Van Loon, J.M. Soler, A. Jakob, M.H. Bradbury, Appl. Geochem. 18 (2003) 1653.
[16] M. Jullien, E. Kohler, J. Raynal, O. Bildstein, Oil & Gas Sci. Technol. – Rev. IFP 60 (2005) 107.
[17] F. Foct, J.M. Gras, in: D. Féron, D. MacDonald (Eds.), Prediction of the long term corrosion behaviour in nuclear waste systems, European Federation of Corrosion Publications 36, Maney Publishing, UK, 2003, p. 91.
[18] C. Pozo, O. Bildstein, J. Raynal, M. Jullien, E. Valcke, Appl. Clay Sci. 35 (2007) 258.
[19] N. Godon, S. Gin, Y. Minet, B. Grambow, K. Lemmens, M. Aertsens, EC report NFPRO-RTDC1-D1.1.1, 2005.
[20] V. Phillipini, A. Naveau, H. Catalette, S. Leclercq, J. Nucl. Mater. 348 (2005) 60.
[21] N. Godon, personal communication.
[22] L. Trotignon, A. Didot, O. Bildstein, V. Lagneau, Oil & Gas Sci. Technol. – Rev. IFP 60 (2005) 107.
[23] J. Cama, J. Ganor, C. Ayora, A.C. Lasaga, Geochim. Cosmochim. Acta 64 (2000) 2701.
[24] E. Busenberg, C.V. Clemency, Geochim. Cosmochim. Acta 40 (1976) 41.
[25] K.G. Knauss, T.J. Wolery, Geochim. Cosmochim. Acta 50 (1986) 2481.
[26] J.D. Rimstidt, H.L. Barnes, Geochim. Cosmochim. Acta 44 (1980) 1683.
[27] L.N. Plummer, D.L. Parkhurst, T.M.L. Wigley, in: E.A. Jenne (Ed.), Chemical modeling of aqueous systems, ACS Symposium Series 93, 1995, p. 412.
[28] G. Kamei, H. Ohmoto, Geochim. Cosmochim. Acta 64 (2000) 2585.
[29] S.A. Carroll-Webb, J.V. Walter, Am. J. Sci. 290 (1990) 797.
[30] P.M. Dove, Geochim. Cosmochim. Acta 63 (1999) 3715.
[31] P.S. Sidhu, R.M. Gilkes, A.M. Cornell, A.M. Posner, J.P. Quirck, Clays & Clay Miner. 29 (1981) 269.
[32] E. Busenberg, L.N. Plummer, Am. J. Sci. 282 (1982) 45.